Re-adjustments for MOM calculations of microstrip and stripline power dissipation

Frederick Huang

Department of Electronic, Electrical and Systems Engineering, University of Birmingham, Edgbaston, Birmingham, B15 2TT, UK

Abstract

Microstrip and stripline losses in Method of Moments (MOM) calculations have an error arising from the large current density at the strip edges, characterized by an integration limit ($W/2\text{-}d$) in the equation for current density in thin strips (width W), where d is a fitting parameter. It depends primarily on the width of the MOM subsection on the edge of the strip. By comparing with the integration limit ($W/2\text{-}\Delta$) for an actual strip with finite thickness, a correction factor is estimated. The equations incorporating d are confirmed by comparing with MOM calculations of isolated stripline, uniformly spaced parallel strips, striplines and microstrips close to ground planes, and with a strip in a uniform, externally applied magnetic field. The results are also consistent with measurements with copper. This makes the accuracy of the loss estimates commensurate with the excellence of the other aspects of MOM simulations.

CAMBRIDGE
UNIVERSITY PRESS

Introduction

In a uniform, zero-thickness isolated stripline, the normalized current density $J(x)$ has the form

$$J^2(x) = \left(\frac{2}{\pi}\right)^2 \frac{1}{(W/2)^2 - x^2},\tag{1}$$

where W is the width of the strip and x is the position, measured from the center of the strip (Fig. 1(a)), as given in Appendix A for $W/2 = 1$. It has the same form as the charge density [1]. Power loss depends on the integral of this function, which has singularities at $x = \pm W/2$, because the finite thickness t of the strip has been ignored. For a thick strip, currents flow on the top, bottom, and side surfaces because of the skin effect, and the 90° corners do not have this singularity.

The singularities are avoided by integrating only within a range $-(W/2) + \Delta < x < W/2 - \Delta$, where fitting parameter Δ is chosen as follows. In Fig. 1(a), $s = x + W/2$, that is, s is measured from the left-hand edge and $s \ll W$. At a 90° corner, the thick-metal current density squared $J_m^2(s)$ increases only as $s^{-2/3}$ instead of s^{-1}, as s decreases. When the two curves shown have equal integrals, the power dissipation per unit length for the finite-thickness strip with surface resistance R_s can be represented by the thin-metal case, $P_\Delta = 4R_s \int_0^{W/2-\Delta} J^2(x)dx$, considering the right-hand half of the top surface, and then multiplying by 4 for the whole strip. The value of Δ, sometimes called the "stopping point" [2] or "stopping distance" [3], is $t/290$ for perfect conductors [4], typically $t/150$ to $t/250$ for finite conductor skin depths as confirmed in experiments [2], and $t/130$ for superconductors [3] in one example [5]. Losses can also be obtained from thick-layer simulations [6, 7] and are also considered in [8–11].

One version of the Method-of-Moments (MOM) [12] uses thin conductors as an approximation and approximates $J^2(s)$ as rectangular basis functions, shown in Fig. 1(b). The combination of rectangles does not account for the singularity of $1/s$ and furthermore, for the second rectangle onwards, the discrepancies between the rectangle functions and $1/s$ may not exactly cancel. The aim of this work is to establish an integration limit ($W/2-d$) such that $P_d = 4R_s \int_0^{W/2-d} J^2(x)dx$ is the MOM estimate of power loss. The ratio P_Δ/P_d becomes the correction factor for simulations. It is useful because the power loss, which is proportional to $J^2(x)$, is particularly sensitive to errors in $J(x)$. The derivation for d is straightforward, but the assumptions are not very obvious, so the bulk of the effort is to confirm that P_d is a fair estimate of $P_{sim} = 4R_s \sum_n J_n^2 X_n$ from actual MOM calculations (with notation from Fig. 1(b)).

The expressions for Δ are already experimentally confirmed in [2]. The present work proposes and confirms the value of d, a numerical exercise. Both a manual MOM procedure and commercially available software Sonnet® [13] are used, for several configurations: isolated stripline; uniformly spaced parallel strips; microstrips and striplines close to ground planes; and strips in a uniform, externally applied magnetic field. Isolated stripline is the simplest case, relevant because the edge singularities are not strongly affected when ground planes are
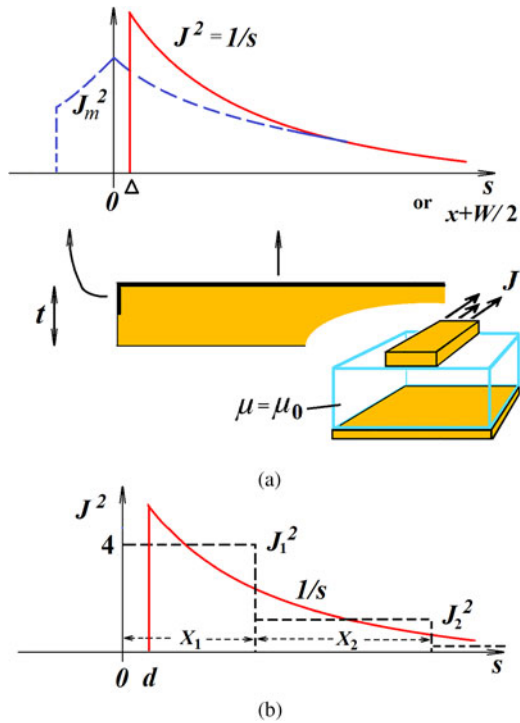
Fig. 1. Fitting parameters: integration limits Δand d for (respectively): (a) strip with finite thickness, and (b) MOM calculation with a zero-thickness conductor.

added, as confirmed by comparison with a microstrip where the substrate thickness is only half the strip width. Coplanar line, in which currents in the adjacent ground planes are in the opposite direction to the center line, are similar to the parallel strips with currents in adjacent lines in the opposite direction. The thick metal calculations and experiments [2] are supplemented by some additional simulations and experimental results to illustrate the calculation process. The comparisons also reveal some features of microstrips which might not be expected, such as a very significant loss under-estimate for coarse meshing.

The MOM calculation (existing software) already gives the overall current distribution, taking into account any dielectrics in the layout. The additional adjustment for the current crowding (this work, characterised by d) is assumed to be independent of the dielectrics, so free-space configurations are considered. This is because, for localized currents, Ampere's law (Appendix B) can be used instead of Maxwell's equations. Supplementary simulations on spirals and meander lines, and experiments with microstrips confirm that the results are still applicable when dielectrics with high relative permittivity ($\varepsilon_r \sim 10$) are present.

For comparison, existing papers [2, 8–11] give stand-alone calculations for P_Δ, using extensive computations with software which does not appear to be intended for arbitrary filter shapes, that is, not simulation software. For the present work, the overall current distribution is found by existing MOM software, requiring only the very localized adjustment to find P_d. Despite being defined by similar equations, P_Δ and P_d are not the same quantity and are not compared to find the error level in one or the other. Instead, previous work [2] is accepted and used in the correction factor P_Δ/P_d, which can be inserted into the software by entering a modified value of metal resistance. The differences and relative merits between [2,8–11] and the MOM itself

[12,13] are not part of the current study. The main advantage is that the improvement in the MOM can be used for complex shapes in filters such as step-impedance hairpins, with very little additional effort.

Evaluation of the integration limit

Using Fig. 1(b), in which the current density (omitting a constant, for clarity) is $J(s) = 1/\sqrt{s}$ so the mean value of $J(s)$ (not $J^2(s)$ as illustrated) between $s = 0$ and $s = X_1$ is given by

$$X_1 J_1 = \int_0^{X_1} \frac{1}{\sqrt{s}} \, ds = 2\sqrt{X_1} \ , \tag{2}$$

$$J_1^2 = 4 \ /X_1. \tag{3}$$

For the rectangular function $J_1^2 = 4/X_1$ and the curve $J^2(s) = 1/s$ (for $s = d$ to X_1) to have equal areas and therefore to represent the same power loss,

$$R_s X_1 J_1^2 = R_s \int_d^{X_1} \frac{1}{s} ds \ , \tag{4}$$

where R_s is the surface resistance, taken to be very small so that it does not affect the current distribution, so

$$d \approx \frac{X_1}{54.6}. \tag{5}$$

This simple equation is the centerpiece of the present work. The second rectangular function with height J_2^2 underestimates $1/s$ for s slightly greater than X_1, causing the MOM equations to over-estimate J_1 and the crowding factor, as will be investigated numerically.

The estimate for the MOM value of power dissipated per unit length of a strip is approximately

$$P_d = 4R_s \int_0^{W/2-d} J^2(x) \, dx \ . \tag{6}$$

For a uniformly distributed current, it is

$$P_u = \frac{2}{W} 4R_s I^2, \tag{7}$$

where I is the current in the top surface of the right-hand half of the strip, which has width $W/2$. Hence an approximate equation for the current crowding ratio included in the MOM is

$$\eta_d = \frac{P_d}{P_u} = \frac{W \int_0^{W/2-d} J^2 dx}{2 \left(\int_0^{W/2} J \, dx \right)^2}. \tag{8}$$

The actual MOM current crowding in simulations is (with notation given in Fig. 1(b))

$$\eta_{sim} = \frac{W \sum_n J_n^2 X_n}{2 \left(\sum_n J_n X_n \right)^2}. \tag{9}$$

Isolated strips

Using $J^2(x)$ for an isolated strip given in Appendix A, with width adjusted from 2 units to W,

$$\eta_d \approx 0.1405 - 0.2026 \ln\left(\frac{2d}{W}\right), \tag{10}$$

for small d. The actual current crowding factor η_Δ for thick conductors based on [4] is the same equation but with d replaced by Δ and the correction factor $\int_0^{W/2-\Delta} J^2(x)dx \,/\, \int_0^{W/2-d} J^2(x)dx$ is equal to η_Δ / η_d (much simpler than η_Δ / η_{sim}). Although η_d and η_Δ share the same equation and the same red line, simulations are likely to have X_1/W between 0.05 and 0.25, on the right-hand half of the graph, while real filters will usually have Δ/W on the left-hand side, so η_Δ / η_d can be substantial, typically 1.5–2.0.

Figure 2 also compares η_d with η_{sim} from manual MOM calculations as given in Appendix B, revealing only a slight variation, believed to be due to the variable-ratio $X_2{:}X_1$. Here, η_d is a function of d, while η_{sim} is a function of X_1, and the agreement shows that the relation (5) is valid. Commercially available software Sonnet® [13] was also used. A uniform, straight strip of width 40 µm is placed in a $2 \times 2 \times 2\ \text{mm}^3$ enclosure, and excited at 1 GHz. Exceptions are for $X_1/W = 0.002$, where $W = 100\ \mu\text{m}$, which illustrate that scaling does not affect the results. Current density plotted by the software is manually read off, and (9) evaluated. Results are also given in Fig. 2(a), with good agreement with the manual MOM and (10). The horizontal discrepancy between the η_d and η_{sim} lines is about 20%, but with the logarithmic relationship, the vertical discrepancy is only about 3%, slightly more for large X_1/W where the approximation $J(s) = 1/\sqrt{s}$ breaks down. It is the vertical separation that is relevant in calculations. Transmission line loss also depends on R/Z_0, where R is the resistance per unit length and Z_0 the characteristic impedance. Because the MOM slightly overestimates the characteristic impedance, there is a small additional error, ignored here but found in some example calculations to be of the order of 2%.

Narrow subsections are usually used near the strip edges where the current density varies rapidly, and larger subsections in the middle. In Sonnet, a default ratio $X_1{:}X_2{:} X_3{:} X_4, \ldots$ is 1:2:4:8…, working inwards, except for the subsections near the center, which are chosen so that the total width is the strip width. This ratio is used in Fig. 2(a), with two values using 1:6:12 … for comparison. Other ratios are shown in Fig. 2(b) where (10) is subtracted so the discrepancy can be greatly magnified. The values of η_{sim}- η_d for the ratios 1:1:1:1 and 1:2:4:8, are very close, implying that the sizes of inner subsections are virtually immaterial. However, comparing 1:2:4:… with 1:6:12…, there is a significant difference. The widths of the inner subsections in corresponding positions are similar; for example, x_3 has a magnitude between X_4 and X_5 (not X_3), as shown in Fig. 2(c). Thus, only the widths of the first and possibly the second subsections are significant. This is re-confirmed with the plots of η_{sim}- η_d for 1:1:m:2m, which also show little change when X_1 and X_2 are not varied.

Parallel striplines

Equations for current density are given in Appendix A for parallel strips, with the currents either all in the same direction or "anti-parallel", alternating in the direction in neighboring strips. The widths and the spaces are both 40 µm. For the anti-parallel strips,
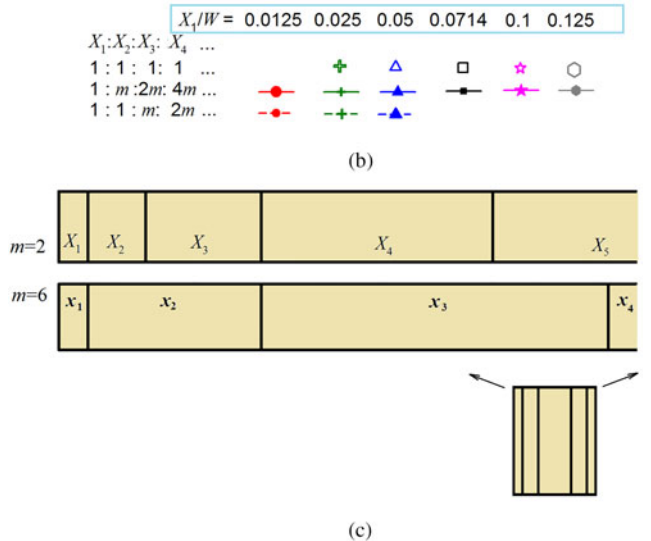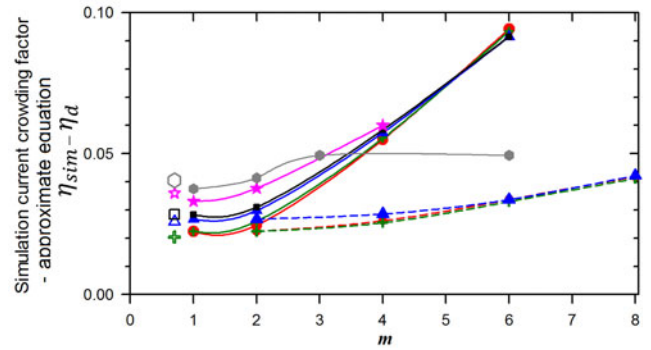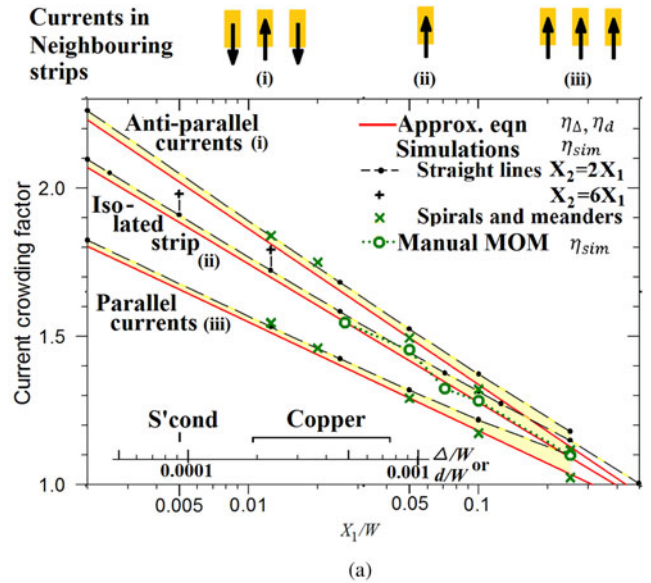
Fig. 2. Current crowding factor: approximate equation (10) compared with MOM calculations (9). For strips carrying a known current. (a) For sub-sectioning $X_1{:}X_2{:}X_3{:}X_4 =$ 1:2:4:8 : typical values of X_1/W for copper and superconductor are given. Red and dashed black lines correspond to the similar lines in Fig. 1. (b) For various values of $X_1{:}X_2{:}X_3{:}X_4$; with the approximate equation subtracted. For 1:1:1:1, m is irrelevant, so the value shown on the graph is arbitrary. (c) Comparison of sub-sectioning: $X_1{:}X_2{:}X_3{:}X_4 = $ 1:2:4:8 and $x_1{:}x_2{:}x_3{:}x_4 = $ 1:6:12:24.

the neighbors were represented by the image currents in the walls of a very narrow box. For the parallel strips, the strip under test was next to a symmetry plane with 32 neighbors on one side

Fig. 3. Resonators used in simulations: one spiral and the other including a meander line, used separately or together.
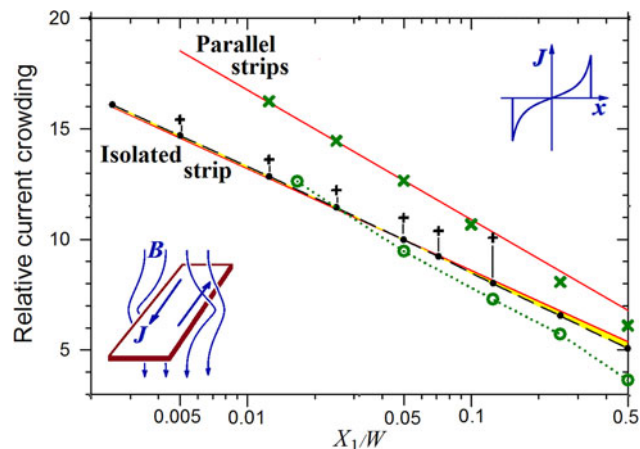

Fig. 4. Current crowding factor estimated from the approximate equation compared with MOM calculations: externally applied uniform magnetic field. (Legend as in Fig. 2 (a).) Red and dashed black lines correspond to the similarly-colored lines in Fig. 1.

and 33 images in the symmetry plane, on the other side. The results, in Fig. 2(a), also show very good agreement.

To observe non-idealized situations instead of straight transmission lines in air, simulations were also done for spirals and meander lines. One case was a spiral similar to Fig. 3, with input and output lines, omitting the other resonator, a meander line combined with an interdigital capacitor (IDC). In the second case, the meander/IDC was provided with nearby input and output lines, and the spiral was omitted. In the fundamental resonance of the spiral [5], currents in adjacent turns are in the same direction, while for the meander/IDC, the current is largest in the meander line, where currents in adjacent sections are anti-parallel.

The substrate has a relative permittivity 9.65 and thickness 0.5 mm, representing MgO (Magnesium Oxide). Line width is 50 μm. The spiral is a 2 mm square with a 3.7 mm tail. The original study was for superconductors [5], but for easier evaluation of bandwidth and quality factor, the surface resistance was entered as 4.6×10^{-4} ohms per square, approximately 100 times that of a typical YBCO superconductor at 2.3 GHz and 20 K with top and bottom surfaces in parallel. For the meander line, it was 8.1×10^{-4} ohms/square, approximately 20 times that of YBCO at the 10 GHz resonance. Losses are estimated from the 3 dB bandwidths of the S_{21} response, giving allowance for the input and output loading found from a re-simulation with zero resonator loss. They are scaled to fit the η_d curve at $X_1/W = 0.05$; there is a close match, except near $X_1/W = 0.5$, where $\eta_d = 0.881$ and 0.928 for the parallel and anti-parallel strips, respectively. Had the values been scaled to $\eta_d = 1$ at $X_1/W = 0.5$, the curves would have been higher. The cause is probably the skewed current distribution and transverse currents near the bends, which introduce more loss in both the simulations and in the thick films. Since only the ratio η_Δ / η_d is required, the curves are confirmed except for extremely coarse mesh.

Strips in a uniform field

When an external uniform perpendicular magnetic field induces a current in the isolated strip, the induced current is also concentrated at the edges (insets, Fig. 4). The conformal mappings, MOM calculation and the simulation layout with a nearly-uniform field are given in Appendices A–C. A non-idealized configuration for simulation is shown in Fig. 3. The lossless spiral, resonating at 2.3 GHz, creates a magnetic field which induces current in the meander/IDC resonator, which has surface resistance 4.6×10^{-4} ohms per square, as before. The second resonator is not resonant at this frequency but loads the spiral. The current density is approximately anti-symmetric, as sketched in the inset of Fig. 4 and in Fig. 13(c). Resonance 3 dB bandwidths are very narrow, but the surface resistance cannot be increased much further without perturbing the current distribution. Very good agreement between the approximate equation, the MOM calculations, and the meander line simulations is shown in Fig. 4. As before, the meander line data are scaled to fit at $X_1/W = 0.05$.

The resonator combination is intended for other work, where the meander resonator attenuates the third-order resonance of the spiral, as in [14–17].

Microstrips and striplines with ground planes

At microwave frequencies, the current is confined to the upper and lower surfaces of the microstrip. With a nearby ground plane underneath, the current density is greater on the microstrip lower surface because of the larger magnetic field, studied by modeling the top and bottom surfaces as two separate layers with a very thin gap. However, in most simulations, they are combined as one layer, since halving the number of sub-sections may result in an eightfold reduction in computation time. These two cases are given in Fig. 5, where $W = 40$ μm. Ground plane losses [1,18,19], are omitted. The value of η_d is assumed to be close to η_{sim} for separate layers, being determined by the $1/s$ dependence of $J^2(s)$ at the edges, as before, and confirmed in the next section.

Errors arise from conflicting requirements for the separation $t = 0.02$ μm between the upper and lower surfaces of the strip. It should be small to avoid obscuring the variation of η_{sim} with X_1/W. For the isolated strip, which has equal top and bottom currents, the difference between using a single layer or separate layers is due solely to t. The worst error is about 5%. To check if t is too small for other values of h, some strips were re-simulated with three layers enclosing two gaps of 0.02 μm. The middle layer does not have zero current density (as it should) because the rectangle function estimates of currents in the top and bottom layers shield the center layer incompletely. In the absence of the middle layer, the field under the strip would influence the current in the top layer. The center current is greatly reduced with $t = 0.04$ μm, even though η_{sim} changed by much less than 0.1, implying very little effect.

The curves should approach the isolated strip for large h/W. This applies even for $h/W = 0.5$; furthermore, the transition to microstrip occurs only at approximately $h/W = 0.2$. For very
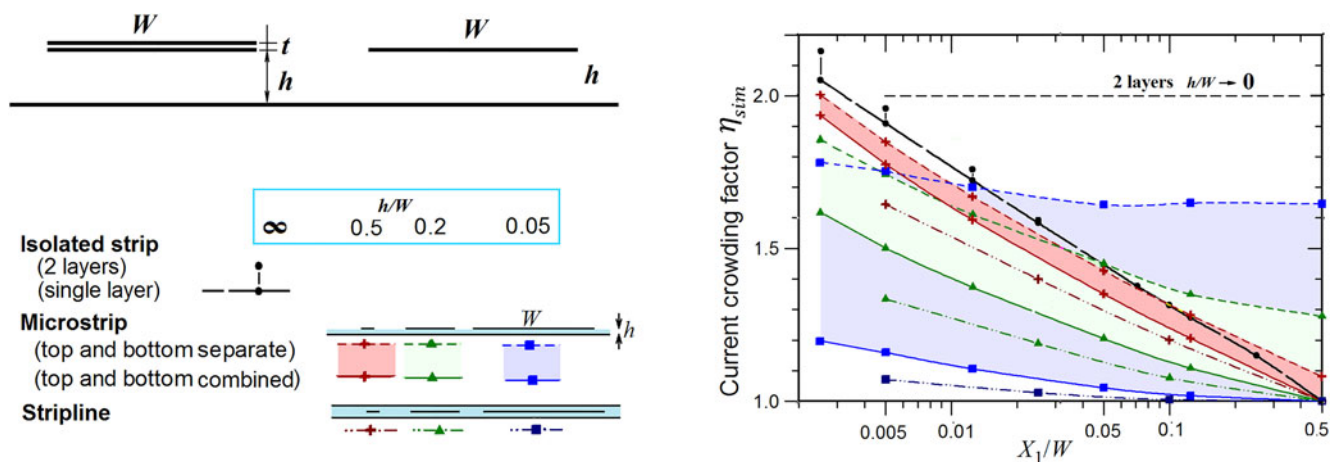
Fig. 5. Current crowding factor for very thin microstrips and striplines, with nearby ground planes, based on MOM (Sonnet) calculations.
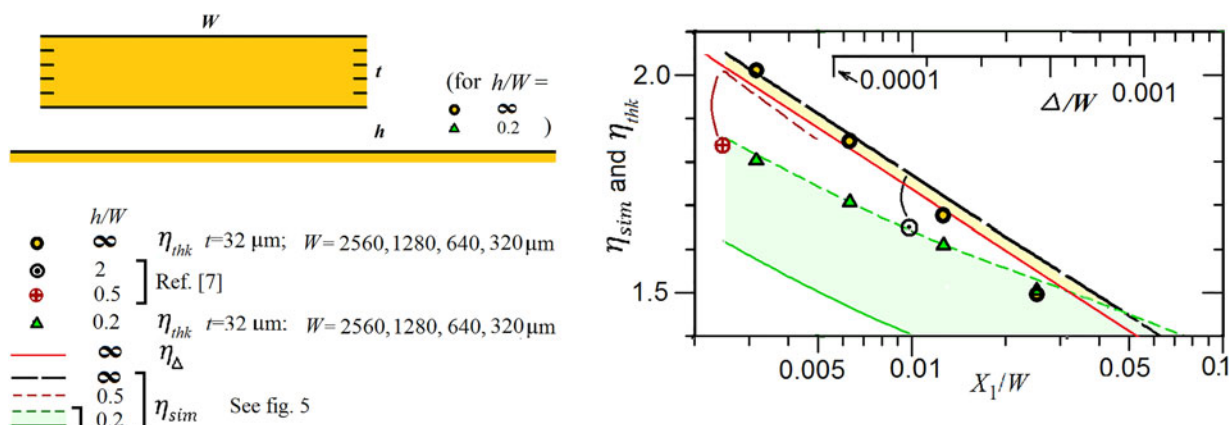

Fig. 6. Current crowding factor for very thick microstrips with nearby ground planes, based on MOM (Sonnet) calculations, $t/2\delta = 16$, compared with the thin-layer simulations.

small h/W it should tend towards $\eta_{sim} = 2$ for the double layer model since current is concentrated on the lower layer, while for a single layer, $\eta_{sim} = 1$. However, for $h/W = 0.05$, $X_1/W \sim 0.125$, the current crowding factor is only about 1.65, showing that a significant current still flows in the top surface. Meanwhile, for $X_1/W \sim 0.005$, all the two-layer curves are near 1.8, giving a reasonable rule of thumb, because current crowding at the edges compensates for the incomplete current crowding between top and bottom.

Turning to striplines, crowding is significant even for $h/W = 0.2$, but less than for the microstrip because more current flows near the center of the top surface, in addition to the bottom surface.

Comparison with thick strips

To supplement η_{Δ} and experimental data in [2], and the additional experimental data in the section "Comparisons with measurements", new simulations for η_{thk} using the thick-layer MOM model was generated for comparison with η_{sim}, the above thin-metal model of 1 or 2 layers. The data are shown in Fig. 6.

X_1/W is sufficiently small so that the current crowding is determined almost exclusively by the thickness. Thus, the horizontal axis for the thin metal is X_1/W, but for the thick metal it is Δ/W, and agreement between the two cases confirms the relation (5). Data are given for $h/W \rightarrow \infty$ and $h/W = 0.2$; $t = 32\,\mu m$, resistivity is $4.31 \times 10^{-9}\,\Omega m$ (a quarter of room-temperature copper), and frequency is 1.092 GHz, to make the skin depth $\delta = 1.0\,\mu m$, that is, much thinner than t. Nevertheless, the skin depth is represented approximately using the appropriate skin resistance and reactance in the thin layer model for each of the top and bottom surfaces, while the side walls were 1 μm wide stacks of thin layers (that is, the software's thick-layer model) with 1 μm gaps. This stack has a rectangular function for a current density of width δ, instead of the exponential profile, but the skin resistance and field penetration are approximately correct. Box length is 100 μm, while other dimensions are much smaller than a wavelength. In this section, the crowding factor was found by comparing S_{21} with the corresponding value of a thin-film reference line with $X_1 = W/2$, instead of using (9), to avoid manual summation of very many terms. Comparing S_{21} values includes the difference arising from different estimates of characteristic impedance (as
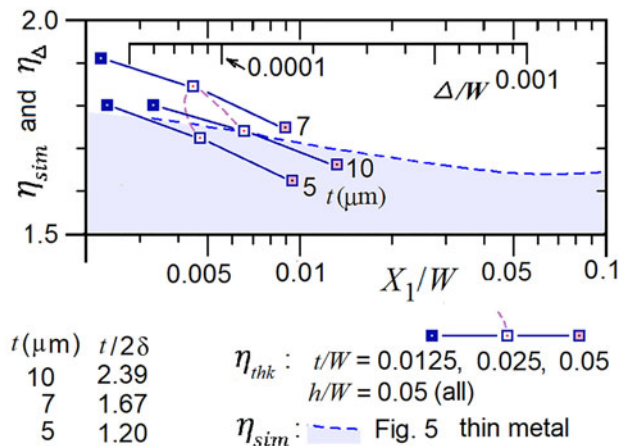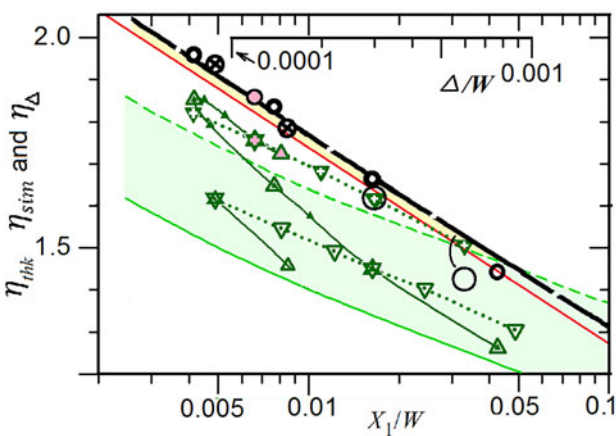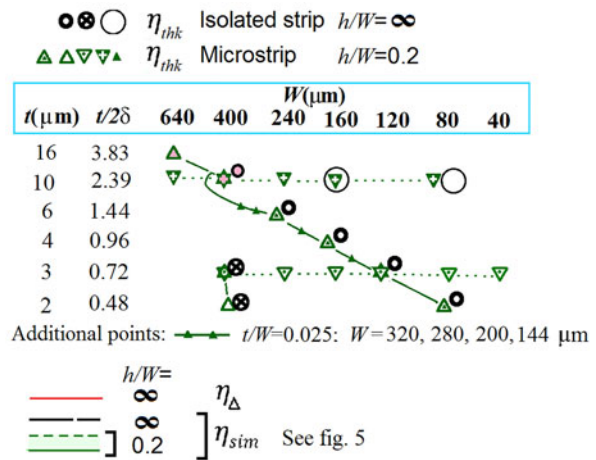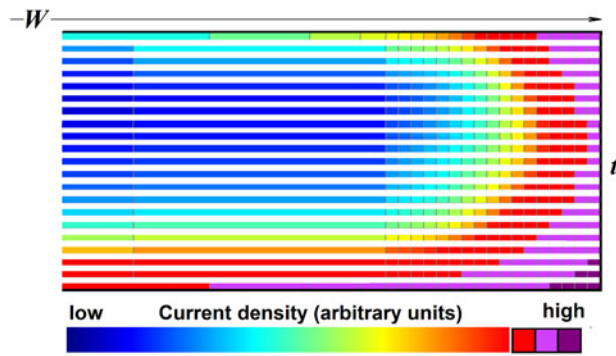
Fig. 7. Current crowding factor for $t/2\delta$ of the order of 1, compared with thin layers.

in the section "Isolated strips"), not considered in (9). The software estimates of characteristic impedance suggest that the difference is particularly large when $h/W = 0.2$, typically 5%.

Figure 6 shows that (5) is a good approximation, except for large t/W, as expected [4] because the conformal mapping there assumes $t \ll W$. Two values of η_{thk} for $t/2\delta = 5.5$ from [8] are also given. Their graphed data have been adjusted by removing dielectric and ground plane losses as given in [1,20]. The point at $X_1/W = 0.00245$ is a consensus of several works which are compared in [9]. For the point at $X_1/W = 0.0098$, h/W is 2 but taken to be infinite since even $h/W = 0.5$ is not very different from $h/W \to \infty$.

In Fig. 7, results are compared with η_{thk} from medium-thickness ($t \sim \delta$) simulations consisting of a stack of thin layers with $t_0 = 0.2$ μm spacing and $W = 40$ to 400 μm, but (because of computer limitations) $t_0 = 0.33$ μm for $W = 640$ μm. Again, $h/W \to \infty$ and $h/W = 0.2$. For resistivity 17.24×10^{-9} Ωm (room temperature copper) and frequency 1 GHz, skin depth is $\delta = 2.09$ μm. Because of the unusually small subsections, several of them are required to resolve the variation of current density near the edge. Eight 1 μm subsections were therefore added, produced in the software by manually drawing narrow touching rectangles instead of one larger rectangle. Maximum t/Δ occurs when $t/2\delta \approx 1.44$ [2], which minimizes Δ. Thus, the series of open circles represents progressively decreasing t, starting with the pink-filled circle; Δ initially decreases and then increases. The same applies to the series of upright triangles.

To find η_Δ, S_{21} loss was compared with a single-layer reference line with $X_1 = W/2$ and sheet resistance

$$R = R_s t \, \mathrm{Im}\left(\frac{\cot(kt) + \csc(kt)}{kt}\right), \qquad (11)$$

based on [2], where R_s is the skin resistance and k is the (complex) wave number within the metal. For $t/2\delta \gg 1$, top and bottom layers are separate and in parallel, so $R \sim R_s/2$, while when $t/2\delta \sim 1$, the skin layers overlap, R is larger, and the reference line is itself affected by the overlapping top and bottom skin layers, but not the current crowding at the edges.

Example series of points with constant t/W, t, and W are given. For $h/W \to \infty$, $t/2\delta > 0.5$, and $t/W < 1/16$, three calculations agree closely:

- η_{sim}, thin-metal simulations together with (5) (broad black line, long dashes);
- η_Δ, where [2,3] give data on t/Δ, which with (10) gives the crowding factor (thin red line); and
- η_{thk}, using the same data on t/Δ but with new thick-metal simulations (black circles).

Admittedly, because of the logarithmic relationship in (10), the horizontal discrepancy, that is, the error in Δ, is larger, but it is
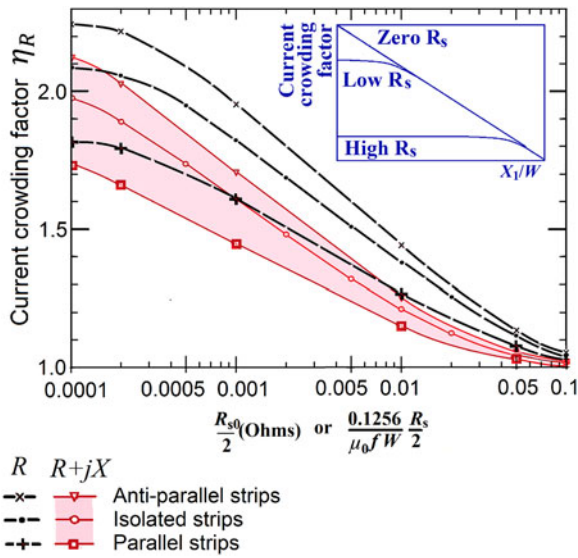
Fig. 8. Current crowding factor for a thin resistive isolated 100 μm wide stripline, based on MOM (Sonnet) calculations.

η_{sim} which is required in calculations. If η_{thk} is accurate, the horizontal shift between it and η_Δ may be due to the approximation that t/Δ in [2] is independent of W. In particular, for the very small and little-used range $t/2\delta < 0.5$ (not shown), η_{thk} and η_Δ agree only for $t/W \sim 1/16$, but here, [2] can be ignored and the thin-metal simulations can be used on their own.

For $h/W = 0.2$, (1) does not apply, but nevertheless, the estimates of η_{sim} are a fair match to η_{thk} for $t/2\delta > 1$. For smaller t, the values of η_{sim} approach the single-layer simulations, as expected, with $t/2\delta = 0.72$ near the center of the transition. For $h/W = 0.05$, the agreement is fair for $t/2\delta > 1.2$.

Thin strips with resistance

Introducing resistance to the thin conductor simulations modifies the current distribution and hence η_d (as it does with the thick model via the parameter $t/2\delta$, previously discussed). The inset in Fig. 8 shows a diagonal line which represents any of the three curves of η_d, the black dashed lines in Fig. 2(a). Strip resistance limits the current crowding factor; moving leftwards, the line reaches a limiting value depending on the resistance. This limit is given in the main figure, obtained in MOM computations. For easier scaling, strip width was changed to 100 μm. The excitation frequency remains 1 GHz. For the parallel strips, there are 16 near neighbor strips included in the calculation on each side of the main strip to reduce computation time. (In two runs with 32 neighbors, the difference is not visible to the scale of the graph). The thin film resistor model was used; for $t/2\delta > 1$, the surface resistance of the top and bottom surfaces in parallel is approximately $R_{s0}/2$, where R_{s0} is the surface resistance for the given 100 μm strip at 1 GHz.

For the same overall resistance, a wider strip has a proportionately larger resistance per unit width. At a higher frequency, the reactance increases, so for a proportionate contribution by resistive and reactive components, the resistance is proportionately larger. Thus, the scaling rule is

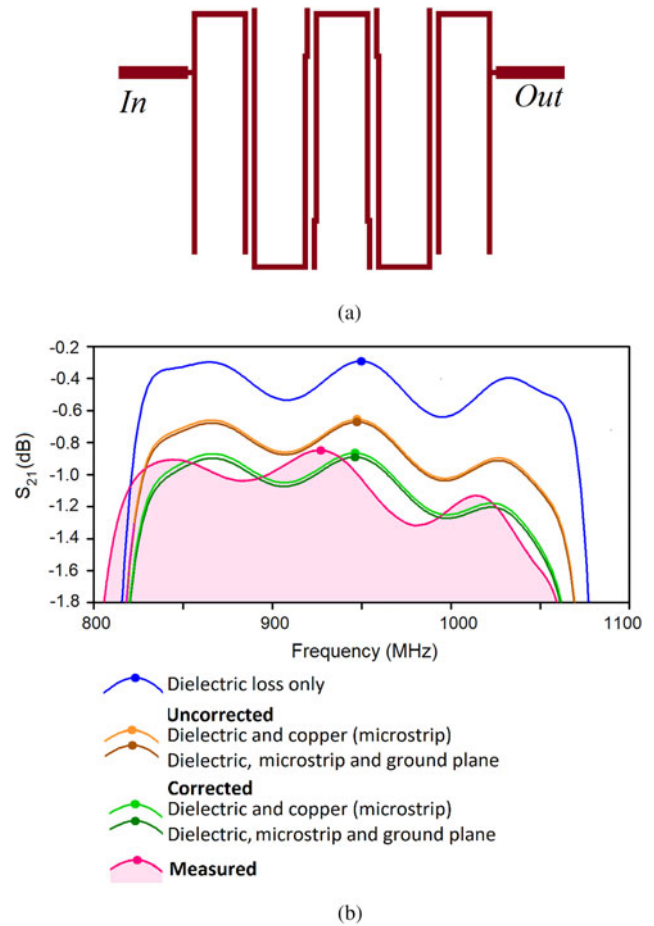$$\frac{R_s}{fW} = \frac{R_{s0}}{10^9 \, 10^{-4}}. \tag{12}$$

Fig. 9. Hairpin filter with 22% bandwidth and 1 GHz center frequency. (a) Layout, (b) simulated frequency response for various loss mechanisms, and measured response.

Alternatively, the horizontal axis $R_{s0}/2$ can be replaced by $(0.1256 / \mu_0 fW) (R_s/2)$ where the permeability of free space μ_0 makes the variable dimensionless and removes the very large constants. To test the scaling, simulations with f and W varied by a factor of 10 made no difference, to within the drawing accuracy. The crowding factor is then the smaller of η_R and η_d, except in the small transition region, where both the finite subsection width and the resistance contribute.

In Fig. 8, $X_1/W = 0.002$ limits η_R as R_s is reduced. Otherwise, the curves would continue to rise to the left, with approximately constant gradient.

Different curves apply when the metal is modeled with a surface impedance of $R + jX$, where $R = X$, as when the skin effect is included, and these are also shown. The appropriate curve depends on the model in the simulation, not on the actual properties of the metal when the aim is to appraise and adjust the MOM loss estimate.

Comparisons with measurements

Two similar hairpin filters, described in [14] for harmonics suppression, were revisited to investigate current crowding; one is shown in Fig. 9(a). They are made with 1.27 mm thick RT Duroid 6010.2 with 18 μm copper thickness. The tracks are 0.5 mm wide, and each resonator is approximately $7 \times 28 \text{ mm}^2$. The manufacturer's latest dielectric data are given in [21]. The external circuits in the simulation and measurement are straightforward: "in" and
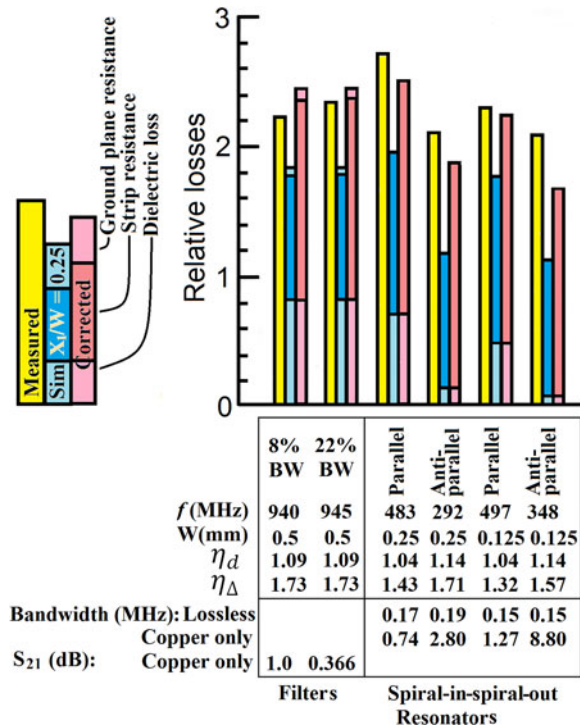
Fig. 10. Losses: measurements compared with computations for microstrip ($h \gg W$) and strips with near neighbors; scaled so that the un-corrected resistive loss ($X_1/W = 0.25$) is 1 unit.

Fig. 11. Resonator to measure losses: (a) precursor: dual spiral resonator. (b) spiral-in-spiral-out resonator. (c) Response.

"out" are connected to source and load, or to ports 1 and 2 of a network analyzer. For one of the filters, simulation results progressively including more and more of the loss mechanisms (dielectric, microstrip resistance, and ground plane) are shown in Fig. 9(b) and compared with the measurement; some of the curves almost coincide. In Fig. 10, the mid-band losses are normalized, dividing by the stated reference value, which is the simulation S_{21} loss for copper only, without the adjustment η_Δ/η_d for current crowding.

Despite the relatively coarse mesh of $X_1/W = 0.25$ in [14], predictions of filter characteristics had been excellent, except for the losses, which required the unrealistic assumption that current only flows on the bottom surface ("current ratio" = 0 in Sonnet) even though current actually flows on both sides when the ground plane is not very close ($h > W$). This is similar to the 1.8 rule of thumb given earlier. The present work shows that η_d is only 1.09, far short of $\eta_\Delta = 1.73$, as estimated from [2]. Taking current to flow on both sides, and including the adjustment η_Δ/η_d, as shown in Fig. 10, substantially improves the loss estimate.

Two further resonators with the same dielectric but no ground plane each comprised two intertwined spirals as in Fig. 11(a) with the inner ends joined as in Fig. 11(b), giving a "spiral-in-spiral-out" resonator with a total of seven turns. The overall dimensions are 10.5×10.5 mm^2 and 7.5×7.5 mm^2, with line widths 0.25 and 0.125 mm, respectively, and $X_1/W = 0.25$. In the fundamental resonance, adjacent turns have anti-parallel currents, while in the second-order resonance, they are parallel. (Meanwhile, the electric fields of the first two resonances probe the dielectric to different depths, so a resonator can also be used to investigate a possible variation of dielectric constant with depth. The double spiral (Fig. 11(a)) is a complementary resonator because the shallow field occurs at the higher resonance instead of the lower frequency.)
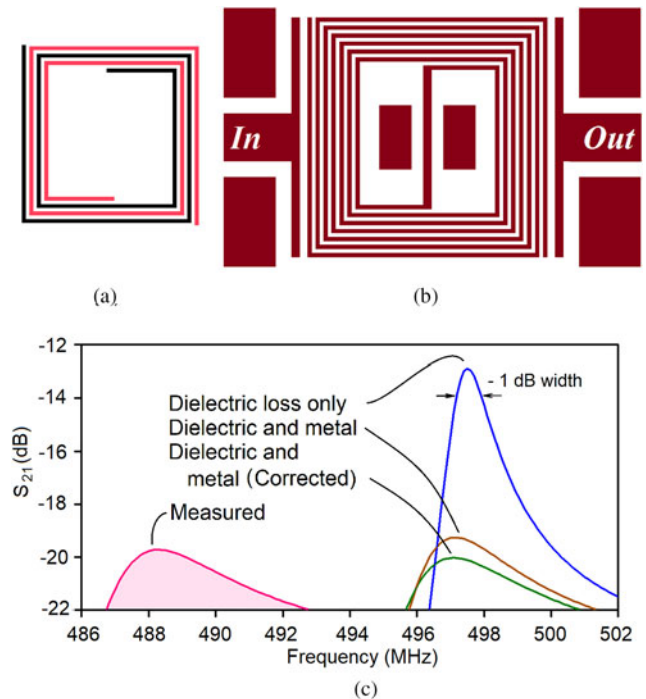
Losses are estimated from the bandwidths of the resonances. Because of a significant skew in the peaks, the 1 dB bandwidth (where $B_{1dB}/f_0 = 1/2Q$) as in Fig. 11(c), instead of 3 dB ($B_{3dB}/f_0 = 1/Q$) was taken, but even so, the losses are not exactly proportional to bandwidth. To make a reasonable comparison (Fig. 10), all losses including the measured loss were based on these bandwidths. The adjusted estimate was obtained by re-simulating with bulk resistance increased by a factor of $(\eta_\Delta/\eta_d)^2$, which increases the surface resistance by η_Δ/η_d because of the skin effect. For a better comparison, the bandwidth for a lossless resonator is subtracted, as it corresponds to a loss in the external circuit. The values are then divided by the bandwidth for the un-adjusted copper loss. It depends on $R/\omega L$, where L and R are the inductance and resistance per unit length of the transmission line; because the magnetic fields in the parallel and anti-parallel cases differ markedly, the normalization factors are also very different.

The bar graph (Fig. 10) shows that this correction again leads to a considerable improvement. The least accurate is for the anti-parallel currents in the strips with 0.125 mm gaps. It may be because the proximity of near neighbors affects the $s^{-1/3}$ dependence of current density near the corners [2], and not only the general distribution described by (1). The strong skew in the frequency response may also have contributed.

Superconductor losses have historically been rather unrepeatable, even with measurements by the same worker at about the same time [22–24]. The same applies to the filter in [5], compared with [25,26], or perhaps the surface resistance has improved by about 25% over the past 20 years.

Conclusion

This work evaluates the error in power loss calculations based on the standard MOM with rectangular basis functions and thin

metal strips, resulting from the incomplete consideration of the concentration of current near the edges. It uses a simple approximation for current density near an edge and compares the result with accepted thick-metal calculations from the literature which are already supported by measurements. The resulting adjustment makes the loss estimates commensurate with the excellence of other MOM results, even with relatively coarse meshing, allowing more complex circuits to be analyzed. Isolated strips and strips with near-neighbors are considered, as is a strip in an externally-applied uniform field. New simulation data with thick metal are also presented. Non-ideal cases with spirals and meander lines, including dielectric layers, are simulated for comparison. For isolated strips ($h/W \rightarrow \infty$), extending down as far as $h/W = 0.5$, an equation is given to estimate the current crowding factor given by MOM calculations of microstrips and striplines. For smaller values of h/W, numerical data are provided. In example calculations with relatively coarse mesh $X_1/W = 0.25$, significant underestimates of η_d were corrected and compared with experiments, showing that the correction factor is valid, while other calculations show that the ground plane is significant only when it is very close to the strip.

References

1. **Collin RE** (1992) *Foundations for Microwave Engineering*. New York: McGraw-Hill Inc.
2. **Holloway CL and Kuester EF** (1994) Edge shape effects and quasi-closed form expressions for the conductor loss of microstrip lines. *Radio Science* **29**, 539–559.
3. **Booth JC and Holloway CL** (1999) Conductor loss in superconducting planar structures: calculations and measurements. *IEEE Transactions on Microwave Theory and Techniques* **47**, 769–774.
4. **Lewin L** (1984) A method of avoiding the edge current divergence in perturbation loss calculations. *IEEE Transactions on Microwave Theory and Techniques. MTT* **32**, 717–719.
5. **Huang F, Bolli P, Cresci L, Mariotti S, Panella D, Lopez-Perez JA and Garcia P** (2018) A superconducting spiral bandpass filter designed by a pseudo-Fourier technique. *IET Microwaves, Antennas and Propagation* **12**, 1293–1301.
6. **Rautio JC and Demir V** (2003) Microstrip conductor loss models for electromagnetic analysis. *IEEE Transactions on\. Microwave Theory and Techniques* **51**, 915–921.
7. **Rautio JC** (2000) An investigation of microstrip conductor loss. *IEEE Microwave Magazine* **1**, 60–67.
8. **Horton R, Easter B and Gopinath A** (1971) Variation of microstrip losses with thickness of strip. *Electronics Letters* **7**, 490–491.
9. **Stracca GB** (1997) A simple evaluation of losses in thin microstrips. *IEEE Transactions on Microwave Theory and Techniques* **45**, 281–283.
10. **Plaza G and Marqués R R** (2006) Medina: quasi-TM MoL/MoM approach for computing the transmission-line parameters of lossy lines. *IEEE Transactions on Microwave Theory and Techniques* **54**, 198–209.
11. **Hamham EM, Mesa F, Medina F and Khalladi M** (2012) Surface-impedance quasi-transverse electromagnetic approach for the efficient calculation of conductor losses in multilayer single and coupled microstrip lines. *IET Microwaves Antennas Propagation* **6**, 519–526.
12. **Harrington RF** (1992) *Field Computation by Moment Methods*. Piscataway, NJ, USA: IEEE Press.
13. 'Sonnet', Available at http://www.sonnetsoftware.com/.
14. **Huang F** (2014) Suppression of harmonics in microstrip filters with stagger tuning and voltage redistributions. *IEEE Transactions on Microwave Theory and Techniques* **62**, 464–471.
15. **Hong S and Chang K** (2006) A parallel-coupled microstrip banpass filter with suppression of both the 2nd and the 3rd harmonic responses. *2006 IEEE MTT-S International Microwave Symposium Digest, San Francisco*, pp. 365–368.
16. **Huang F** (2010) Suppression of superconducting filter spurious response using lossy parasitic resonators. *IET Microwaves, Antennas and Propagation* **4**, 2042–2049.
17. **Huang F** (2011) Suppression of microstrip filter spurious responses using frequency-selective resistive elements. *IET Microwave Antennas and Propagation* **5**, 1836–1843.
18. **Holloway CL and Kuester EF** (1988) Closed-form expressions for the current density on the ground plane of a microstrip line, with application to groundplane loss. *IEEE Transactions on Microwave Theory and Techniques* **54**, 4018–4019.
19. **Holloway CL and Kuester EF** (1988) Corrections to "closed-form expressions for the current density on the ground plane of a microstrip line, with application to groundplane loss. *IEEE Transactions on Microwave Theory and Techniques* **43**, 1204–1207.
20. **Edwards TC** (1981) *Foundations for Microstrip Design*. New York, Wiley.
21. **General information of die1lectric constant for RT/duroid® 6010.2LM & RO3010TM High frequency circuit materials**. Available at http://www.rogerscorp.com/documents/2379/acs/General-Information-of-Dielectric-Constant-for-RT-duroid-6010.2LM-RO3010-High-Frequency-Circuit-Materials.pdf (Accessed September 2014).
22. **Farber E, Deutcher G, Contour J and Jerby E** (1998) Penetration depth measurement in high quality YBa$_2$Cu$_3$O$_{7-x}$ thin films. *European Physical Journal B* **5**, 159–162.
23. **Velichko AV, Porch A, Lancaster MJ and Humphreys RG** (2001) Anomalous features in surface impedance of Y-Ba-Cu-O thin films: dependence on frequency, RF and DC fields. *IEEE Transactions on Applied Superconductivity* **11**, 3497–3500.
24. **Avenhaus B, Porch A and Lancaster MJ** (1995) Microwave properties of YBCO thin films. *IEEE Transactions on. Applied Superconductivity* **5**, 1737–1740.
25. **Semerad R.** Private communication.
26. **Irgmaier K, Semerad R, Prusseit W, Ludsteck A, Sigl G, Kinder H, Dzick J, Sievers S, Freyhardt H and Peters K** (2002) Deposition and microwave performance of YBCO films on techincal ceramics. *Physica C: Superconductivity* **373–376**, 554–557.
27. **Cohn SB** (1955) Shielded coupled-strip transmission line. *IRE Transactions on Microwave Theory and Techniques* **3**, 29–38.
28. https://en.wikipedia.org/wiki/Helmholtz_coil, accessed 28 November 2018.

Appendix A: Conformal mappings for stripline

Conformal mappings [27] for striplines with width $W = 2$ are given in Table 1 and Fig. 12. The complex variable w in the conformal mappings is not to be confused with W. For unity current density in the t-plane, the normalized power dissipated in the right-hand half of a strip is

$$\eta_d = \int_0^{1-d} J^2(x)dx = \int_0^{1-d} \left|\frac{dt}{dz}\right|^2 dx. \tag{A.1}$$

Results are given for $d \ll 1$. The strips are either isolated or have 1:1 mark-to-space ratio. The "parallel" strips have currents in the same direction while for the "antiparallel" strips, currents in adjacent strips are in opposite directions.

The vertical walls in the z-planes do not exist in the actual structures but are inserted so that the fields in the region $|Re(z)| < 2$, $Im(z) > 0$ in Figs 12(b) and (d) or $|Re(z)| > 0$ in Fig. 12(c) are appropriate.

Transform 2 for the anti-parallel strips arises from the Schwartz–Christoffel transformation [27], and since the total current on the right-hand half of the strip is 1,

$$K = \int_0^1 \frac{1}{\sqrt{1-w^2}\sqrt{1-w^2/2}}dw, \tag{A.2}$$

found in tables of the complete elliptic integral to be 1.854.

Table 1. Conformal mappings for current crowding factor η_d

Configuration	Transform 1	Transform 2	$J = \left\|\frac{dt}{dz}\right\|; \frac{dt}{dz} =$	$\eta_d =$
Strips carrying current				
Isolated	No transform i.e. $w = z$	$t = \frac{2}{\pi} \operatorname{asin}(w)$	$\frac{2}{\pi\sqrt{1-w^2}}$	$0.1405 - 0.2026 \ln(d)$
Parallel	$w = \sqrt{2}\sin\left(\frac{\pi}{4}z\right)$	$t = \frac{2}{\pi}\operatorname{asin}(w)$	$\frac{\cos(\pi z/4)}{\sqrt{2\cos(\pi z/2)}}$	$0.2884 - 0.1592 \ln(d)$
Anti-parallel	$w = \sqrt{2}\sin\left(\frac{\pi}{4}z\right)$	$\frac{dt}{dw} = \frac{1}{K\sqrt{1-w^2}\sqrt{1-w^2/2}}, \quad K = 1.854$	$\frac{1}{7.416}\frac{\pi\sqrt{2}}{\sqrt{\cos(\pi z/2)}}$	$0.0552 - 0.2284 \ln(d)$
Strips in externally applied uniform magnetic field				
Isolated	$w = z^2$	$t = \sqrt{w-1}$	$\frac{-jz}{\sqrt{1-z^2}}$	$-2.614 - 2\ln(d)$
Parallel	$w = \sqrt{2}\sin\left(\frac{\pi}{4}z\right)$	$t = \frac{2}{\pi}\operatorname{asin}(w)$	$\frac{\cos(\pi z/4)}{\sqrt{2\cos(\pi z/2)}}$	$-3.385 - 2.546 \ln(d)$
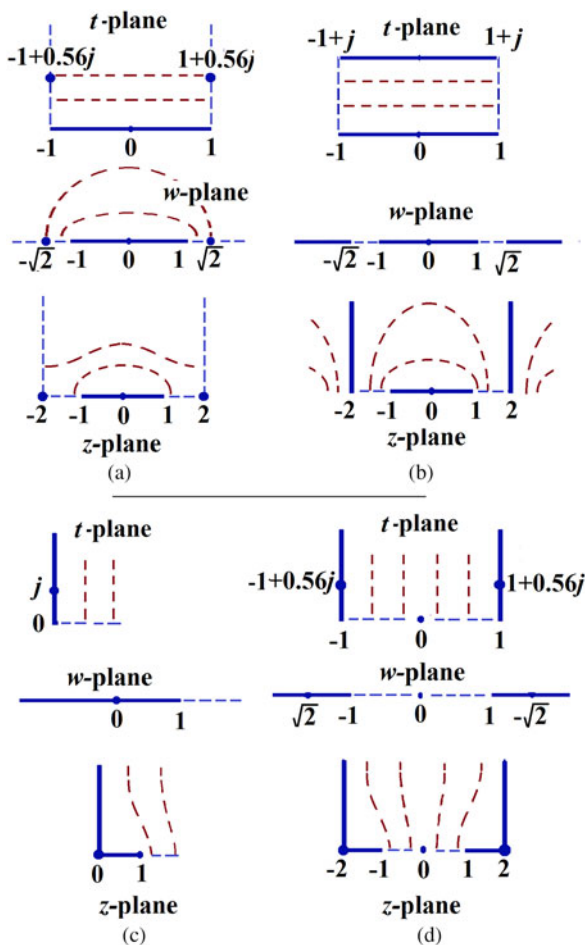
Fig. 12. Conformal mappings for stripline. (a) An isolated strip, or parallel strips with all currents in the same direction. (b) Parallel strips with current directions alternating. (c) An isolated strip in an externally applied uniform field. (d) Parallel strips in an external field.

For the strips in an external field, a factor of 2^2 is added to allow for current in both sides of the strip, while in Fig. 12(d), there is a further factor of 2^2 to re-normalize the flux density in the z-plane at large $Im(z)$.

For the parallel strips in an external field, the limits of integration in (A.1) are $1 + d$ to 2.

Appendix B: The method of moments

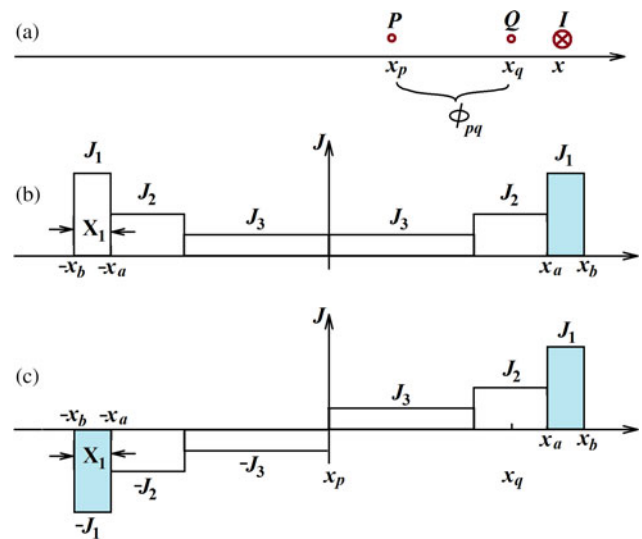By Ampere's law, a long, straight wire at point x carrying a current I results in a magnetic flux density

$$B = \frac{\mu_0 I}{2\pi r}, \tag{B.1}$$

where r is the distance from the wire (Fig. 13). Integrating between points P and Q,

$$\varphi_{pq} = \frac{\mu_0 I}{2\pi}\ln\frac{x - x_p}{x - x_q}, \tag{B.2}$$

so in Fig. 13(b), integrating between x_a and x_b where the constant current density is J_1, it is

$$\frac{2\pi}{\mu_0}\varphi_{pq} = J_1\{(x_b - x_p)\ln|x_b - x_p| - (x_b - x_q)\ln|x_b - x_q| \\ - (x_a - x_p)\ln|x_a - x_p| + (x_a - x_q)\ln|x_a - x_q|\} \tag{B.3}$$

Fig. 13. Method of moments calculation using piecewise constant approximations (rectangular functions). (a) Magnetic flux φ_{pq} in a zone PQ due to a current I. (b) Current distribution in a stripline carrying a current. (c) Current distribution in a stripline in an externally applied uniform field.

Similar terms for the other five rectangular current distributions are omitted for clarity.

In this version of the MOM, P and Q are at the centers of the rectangular functions on the right-hand half of the strip. By taking various points for P and Q, N-1 independent equations can be formulated for N unknown values of J_n; attempting to take more combinations leads to non-independent equations. Flux penetration φ_{pq} within the strip is zero. The total current on the right-hand half of the strip is

$$I_{tot} = X_1 J_1 + X_2 J_2 + X_3 J_3 . \tag{B.4}$$

There are enough equations to solve for J_1, J_2, and J_3 in terms of I_{tot}. This is easily adapted for fewer rectangular functions, but with more than three unknowns, using a pocket calculator is very tedious and general-purpose mathematical software such as MathCad, Matlab, Mathematica or "C" would be required.

For an externally applied field (Fig. 13c), φ_{pq} is equal but opposite to that field, making the total zero. Taking $x_p = 0$ and *two* symmetrically placed rectangular functions,

$$\frac{2\pi}{\mu_0}\varphi_{pq} = J_1\{(x_b + x_q)\ln|x_b + x_q| - (x_b - x_q)\ln|x_b - x_q| \\ - (x_a + x_q)\ln|x_a + x_q| + (x_a - x_q)\ln|x_a - x_q|\} \tag{B.5}$$

Again, similar terms for J_2 and J_3 should be included, but there is no equation for I_{tot} since it is always zero with the anti-symmetric current density.

Appendix C: Uniform applied magnetic field

A nearly uniform field can be generated in a simulation using Helmholtz coils [28], consisting of two co-axial circular coils of radius and separation both r. The two-dimensional equivalent is an infinitely long rectangle with short side $2l$, shown in Fig. 14 as the two upper strips. Because only the vertical component B_y has to be uniform, the lower coil is omitted. The strip is in a plane $0.55l$ below the plane of the coil. (In a plane $l/\sqrt{3}$ below the coil, B_y is maximally flat up to the x^3 term, while for $0.55l$, the ripple is only $\pm 0.07\%$ and the
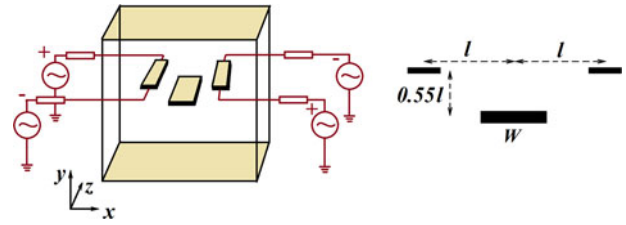

Fig. 14. Approximating a uniform field in simulations: $l = 80\,\mu m$, $W = 40\,\mu m$, and the cubical cavity has side $2000\,\mu m$.

region of nearly constant B_y is larger.) The short $2000\,\mu m$ strip length saves computation time, but it could have been even shorter. It can be shown by Ampere's law that the flux density is given by

$$\frac{2\pi l}{\mu_0 I}B_y \approx 1.536, \tag{C.1}$$

where I is the current in the upper two strips.

Frederick Huang received the B.A. and D. Phil degrees in Engineering Science from the University of Oxford in 1980 and 1984. Since 1989 he has been a lecturer and then an honorary research fellow with the University of Birmingham, UK. Previous research interests are surface acoustic wave (SAW) dot array pulse compressors, analogue voice scramblers, Langmuir-Blodgett films, SAW and superconducting linear phase, and chirp filter synthesis using inverse scattering, slow-wave structures, superconducting quasi-lumped element filters, switched filters and delay lines, together with microstrip and waveguide discontinuities. The main current interests are spiral band-pass filters and filter harmonic suppression.